1 **An *In situ* Method for the High Resolution Mapping of ^{137}Cs and Estimation of Vertical**

2 **Depth Penetration in a Highly Contaminated Environment.**

3

4 Adam Varley[β], Andrew Tyler[β], Mark Dowdall[α], Yuri Bondar,

5

6 [β] Department of. Biological and Environmental Sciences, University of Stirling, Stirling, FK9

7 4LA, United Kingdom

8

9 [α] Norwegian Radiation Protection Authority, Grini næringspark 13, 1332 Østerås, Norway
10
11
12
13
14
15
16
17
18
19
20
21
22
23
24
25
26
27
28
29
30
31
32
33
34

Abstract

The Chernobyl nuclear power plant meltdown has to date been the single largest release of radioactivity into the environment. As a result, radioactive contamination that poses a significant threat to human health still persists across much of Europe with the highest concentrations associated with Belarus, Ukraine and western Russia. Of the radionuclides still prevalent with these territories ^{137}Cs presents one of the most problematic remediation challenges. Principally, this is due to the localised spatial and vertical heterogeneity of contamination within the soil (~10's of meters), thus making it difficult to accurately characterise through conventional measurement techniques such as static *in situ* gamma-ray spectrometry or soil cores. Here, a practical solution has been explored, which utilises a large number of short-count time spectral measurements made using relatively inexpensive, lightweight, scintillators (sodium iodide and lanthanum bromide). This approach offers the added advantage of being able to estimate activity and burial depth of ^{137}Cs contamination in much higher spatial resolution compared to traditional approaches. During the course of this work, detectors were calibrated using the Monte Carlo simulations and depth distribution was estimated using the peak-to-valley ratio. Activity and depth estimates were then compared to five reference sites characterised using soil cores. Estimates were in good agreement with the reference sites, differences of ~25 % and ~50 % in total inventory were found for the three higher and two lower activity sites, respectively. It was concluded that slightly longer count times would be required for the lower activity (<1 MBq m^{-2}) sites. Modelling and reference site results suggest little advantage would be gained through the use of the substantially more expensive lanthanum bromide detector over the sodium iodide detector. Finally, the potential of the approach was demonstrated by mapping one of the sites and its surrounding area in high spatial resolution.

Highlights

• Chernobyl-derived ^{137}Cs poses a risk to human health.

• Highly heterogeneous contamination within tens of kilometres of Chernobyl particularly difficult to characterise.

• Numerous short count time gamma-ray measurements can address spatial resolution issues.

• Peak-to-valley method provides improved depth and activity estimates.

1. Introduction

The accident that occurred at the Chernobyl Nuclear Power Plant (ChNPP) in April 1986 resulted in the radioactive contamination of wide areas of Europe and, to a greater extent, the territories of Belarus, Ukraine and the western Russian Federation. In areas of south Belarus the deposition exceeded 1500 kBq/m^2 ^{137}Cs, 3 orders of magnitude greater than that which resulted from atmospheric nuclear weapons as of 1986 (UNSCEAR, 2000). As a result of the accident, a total area exceeding 60,000 km^2 of forested land was contaminated, including over 20,000 km^2 of the Gomel and Mogilev regions of Belarus in addition to areas near Kiev and in the Russian Federations' Bryansk region. The primary contaminants as a result of the accident were ^{137}Cs, ^{90}Sr and ^{239}Pu. Highest levels of contamination, in excess of 1.4 MBq/m^2 of ^{137}Cs occur with the southernmost parts of the reserves territory over lands nearest the Chernobyl reactor while localised areas of high contamination can be found distributed throughout the reserve. Sr-90 is present at densities up to 3 MBq/m^2 while ^{241}Am levels have approximately doubled over the past twenty years and now approach 0.1 MBq/m^2 in places as a result of ingrowth from ^{241}Pu (Smith and Beresford, 2002). Actinides such as ^{238}Pu and ^{239,240}Pu are present at levels up to 0.037 MBq/m^2 and 0.074 MBq/m^2 respectively. The Polessie State Radioecology Reserve (PSRER) in southern Belarus is one of the most contaminated regions with associated total inventory estimates of 2.5 x 10^9 MBq of ^{137}Cs and 0.18 x 10^9 MBq of ^{90}Sr (Izrael and Bogdevich, 2009). Contamination is spatially highly heterogeneous over distances of 10's of meters or less while significant contamination is also found in the tree canopy and vegetation and in aquatic systems of the area. A general overview of ^{137}Cs levels in the PSRER is presented in Figure 1.

…………………………..Insertion point for Figure 1…………………………………..

Figure 1. Spatial distribution of the estimated ^{137}Cs inventory (kBq m^2) across the Polessie State Radioecology Reserve

Cs-137 is usually considered to be the most important long-term anthropogenic contributor to the dose-levels in the environment (Miller, 2007). Its radiological prominence is due to its relatively long half-life of 32 years, its potential to be remobilised through sediment redistribution as it binds strongly to clays and its affinity to be taken in by living tissue given that it readily displaces biological potassium within the body (Povinec et al., 2003). These

110 factors, amongst others, impart a certain emphasis on the monitoring of levels of this isotope

111 within the environment and such monitoring is especially important in highly contaminated

112 areas such as those of the PSRER where considerable efforts have been expended in

113 establishing the spatial distribution and environmental behaviour of this and other nuclides

114 (see for example Kudelsky,et al., 1996; Knatko et al., 1996; Guermentchuk et al., 1997;

115 Sokolik et al., 2001; Yoschenko et al., 2006).

116

117 Monitoring of ^{137}Cs in soils is conventionally achieved by either of two approaches. The first

118 consists of extracting discrete samples or cores from a site and measuring the activity of either

119 the whole sample or of individually sliced samples representative of different depths using

120 laboratory based gamma-ray spectrometers (Tyler, 2008). Although precise information as to

121 the ^{137}Cs depth penetration can be obtained using this method, the resources it takes to obtain,

122 prepare and count individual samples results in spatial coverage being limited and spatial

123 heterogeneities may not always be captured (Tyler et al., 1996a). Estimates of ^{137}Cs

124 penetration down the soil column are particularly important for two reasons. Firstly,

125 knowledge of depth distribution can contribute greatly to remediation strategies and decisions

126 on subsequent site use. Secondly, depth distribution can influence the environmental

127 behaviour of ^{137}Cs particularly with regards to surface remobilisation.

128

129 The environment of the PSRER constitutes an interesting problem with respect to how high

130 resolution mapping of contaminant ^{137}Cs can be conducted. The territories not covered by

131 forest (basically abandoned agricultural lands) constitute 38.0 % and non-agricultural

132 unforested lands occupy 9.3 %. Road coverage is sparse and the terrain is generally rugged.

133 While topographically flat, the area has local depressions and elevations as well as a variety

134 of watercourses and bodies (both natural and man-made) in addition to extensive seasonally

135 flooded areas. In general, much of the area is inaccessible by vehicle and can be considered as

136 difficult terrain. In light of the above considerations, the development of a man portable

137 gamma-ray spectrometry system capable of accurate high spatial resolution ^{137}Cs mapping of

138 contamination patterns is paramount (Plamboeck et al., 2006). Within the PSRER, due to

139 spatial hetergeneity ^{137}Cs activity the capability to map changes over metres to tens of metres

140 would provide significant improvement in spatial resolution compared to current approaches.

141

142

143

144 *1.1. In Situ Gamma-ray Spectrometry of ^{137}Cs and Depth Estimation.*

145 The fundamentals of gamma-ray spectrometry can be found elsewhere, for example Knoll

146 (2010). The principle of *in situ* gamma-ray spectrometry is the placing of a suitable

147 instrument above the ground and making a measurement over a specified time period. The

148 resultant measurement offers information as to the localised radiation field through the

149 differential measurement of gamma-rays that interact with the active volume of the detector.

150 Critically, the energies of individual gamma-rays are recorded and accumulated into a

151 differential energy spectrum. Estimating the ^{137}Cs inventory (Bq m^{-2}) directly from the count

152 rate under the characteristic ^{137}Cs 662 keV photopeak is not always a straightforward task

153 given that a number of factors can significantly change the count rate. Ground curvature

154 (Laedermann et al., 1998) and the influence of trees and other vegetation (Gering et al., 2002)

155 can introduce a considerable amount of uncertainty. However, the primary source of

156 uncertainty often arises when significant changes in depth distribution are encountered, as

157 considerable variations can alter the count rate by orders of magnitude (Sowa et al., 1989).

158 Besides altering the count rate, changes in depth distribution can also change the detector's

159 Field of View (FoV) and can have an influence on the spatial response of single

160 measurements. The FoV of a detector can be defined as the effective volume of soil being

161 sampled and is often characterised by the lateral distance or radius from the detector over

162 which the sampling area extends to (Tyler et al., 1996a). Problems can arise when

163 contamination is highly associated with the soil surface, following fresh deposition, reducing

164 the detectors ability to resolve small scale localised heterogeneity given that the FoV for a

165 detector at 1 m above the ground is greater than 70 m radius. Moreover, at this scale

166 topographic anomalies become important in defining the FoV. Nevertheless, Chernobyl

167 deposition has aged over 30 years and much of the contamination is understood to have

168 penetrated sufficiently into the soil column (Smith and Beresford, 2002). This process should

169 have led to reduction in the FoV for a detector at 1m above the ground to approximately less

170 than 10 m (Tyler et al., 1996a). A further way to reduce the FoV is to operate detectors at a

171 nominal height of 0.1 m, which should reduce the FoV down to between 2 to 5 m.

172

173 Importantly, prior to any inventory estimations the count rate must be corrected for the

174 appropriate depth distribution and the influence of the FoV must also be considered prior to

175 interpolation mapping. The peak-to-valley ratio (PTV) provides a means of performing this

176 task through spectral information alone (Zombori et al., 1992). PTV has been widely used to

177 estimate the burial depth distribution of ^{137}Cs and improve the overall accuracy of inventory

178 estimations (Feng et al., 2012; Gering et al., 1998; Hillmann et al., 1996; Tyler, 2004). Tyler

179 et al (1996b) puts forward a particularly visual description of the physical processes that the

180 PTV method is developed upon. In summary, the PTV is the ratio between the number of full

181 energy and forward scattered photons (Figure 2). Forward scattered photons are essentially

182 photons that have lost a small amount of energy whilst exiting the soil and can be located in

183 the "valley" region of the spectrum between the full energy peak at 662 keV and the Compton

184 edge at 480 keV (Figure 2b). Importantly, the greater the depth at which a source is present

185 (Figure 2a), the higher is the probability of photons undergoing forward scattering and

186 occupying the valley region, leading to an increase in valley height and a decrease in the PTV

187 (Figure 2c).

188

189 The PTV method can be applied to any detector of adequate energy resolution (Kastlander

190 and Bargholtz, 2005; Tyler, 2004). At present, two of the most commercially widely viable

191 available scintillators that are eminently suitable for portable field operations and that offer

192 high enough energy resolution to measure ^{137}Cs are sodium iodide (NaI:Tl) and lanthanum

193 bromide (LaBr:Ce) (Guss et al., 2010). Of these two, NaI:Tl has been the workhorse of *in*

194 *situ* and mobile gamma-ray spectrometry for a number a decades as it is relatively cheap,

195 robust and provides acceptable energy resolution (~7% at 662 keV). LaBr:Ce on the other

196 hand is a relatively novel scintillator providing superior energy resolution (2.5% at 662 keV)

197 and higher energy efficiency due to its higher density (5.1 g cm^{-3}) compared to NaI:Tl (3.7 g

198 cm^{-3}). LaBr:Ce does contain an intrinsic background component that can deteriorate the

199 signal to noise ratio especially at low count rates (Nilsson et al., 2014). Another key

200 limitation of LaBr:Ce is that it costs almost an order of magnitude significantly more than

201 NaI:Tl. There have been a relatively large number of studies comparing the performance of

202 NaI:Tl and LaBr:Ce through theoretical or experimental means (Guss et al., 2010; Iltis et al.,

203 2006; Milbrath et al., 2007). Nonetheless, limited comparisons have been undertaken in the

204 field (Duval and Arnold, 2013; Nilsson, 2010) and furthermore only a subset of these have

205 pertained to the measurement of ^{137}Cs (Nilsson et al., 2014).

206

207 ………………………………Insertion Point for Figure 2……………………………

208

209 *Figure 2. The relationship between changes in depth distribution (β) and the peak-to-valley*

210 *ratio observed in a 71 × 71 mm sodium iodide detector. A) Normalised depth distributions*

211 *for the same inventory ; B) Peak normalised spectra for different β values demonstrating*

212 *the relative increase in valley counts with increasing burial; C) A straight-forward*

213 *regression between calibrated peak-to-valley ratio and β value.*

214 The overarching aim of this investigation is to compare NaI:Tl and LaBr:Ce detector systems

215 for the purposes of characterising spatial ^{137}Cs contamination including its vertical depth

216 distribution at high spatial resolution using one second acquisition times within the PSRER.

217

218

219

2. Methodology

2.1. Field Sites.

The selected sites within the PSRER were topographically flat over areas of 50 m in diameter, the centre of each site being marked with a square area of the size 100 m². Each site was specifically chosen to be as homogeneous as possible. As a general indicator of the conditions of the site, the gamma dose rate was recorded with an AT6130 Radiation Monitor (Scientific and Production Enterprise ATOMTEX, Belarus) at each corner and in the centre at a height of 1 m and soil samples were taken at the same points. The location and ambient dose rates over the five sites were as follows: Site 1, a soddy podzolic soil at N 51º33′07,9″ E 029º55′26,1″ (2.21 to 2.50 µSv/h); Site 2, a sandy soil at N 51º33′17,1″ E 029º55′12,1″, (0.29 to 0.35 µSv/h); Site 3, an organic peat soil at N 51º32′54,7″ E 029º55′52,2″ (1.55 to 1.73 µSv/h); Site 4, a regularly flooded, mineral floodplain soil at N 51º31′45,2″ E 029º56′07,5″ (0.52 to 0.89 µSv/h); Site 5, a mineral, ploughed soil at N 51º47′11,8″ E 030º01′16,8″ (0.25 to 0.39 µSv/h). A standard cylindrical corer of 4 cm in diameter and 20 cm extent was used to take cores, each divided into the following increments: 0-3 cm, 3-6 cm, 6-10 cm, 10-15 cm, 15-20 cm. All layers of the same depth from the five cores were bulked and homogenized for gamma-spectrometry. The preparation of soil samples for the radioanalytical measurements included air drying and homogenization by mixing and sieving (2 mm aperture). After weighing, a subsample was transferred to the analytical geometry for counting. A HPGe (Canberra, Be5030, carbon fibre window, 50% rel. eff.) detector was used for ¹³⁷Cs determination. Count times varied from 6000 to 80000 sec. Statistical uncertainties for the photo peak of ¹³⁷Cs were less than 5 %. Details as to ¹³⁷Cs contamination levels at the five test sites are provided in Table 1. For further site information and detailed photographs of the sites refer to Dowdall et al., (2015).

2.2. Gamma-ray Spectrometry System

A 71 (Ø) × 71 mm NaI:Tl and 71 (Ø) × 71 mm LaBr:Ce detectors (both made by Saint Gobain) were connected to individual Ortec digiBases recording a 1024 channel spectral every second using Ortec's Maestro software (ORTEC, 2005). Accompanying each spectrum, GPS coordinates were recorded using an SX Blue II differential GPS, with a resolution of 0.6 m. The software used to combine spectral measurements and spatial coordinates was built

251   within the JAVA framework and was able to provide real-time feedback on count rates in

252   specified windows. To avoid significant spectral drift occurring, Maestro's gain stabilisation

253   software was operated on the 662 keV peak. In order to capture local inhomogeneities, the

254   detectors were to the operators best abilities held at a constant height of 0.1 m from the

255   ground at all times to narrow the field of view. This was expected to deviate by 0.1 m either

256   way. The shape of the spectrum was assumed not to change significantly therefore, only the

257   count rate was altered according to the changing field of view and calculated through a

258   deterministic model; this was built in as an uncertainty following Monte Carlo simulations. A

259   walking speed of approximately 0.5 m s^{-1} and transect spacing of 0.5 to 1 m was maintained

260   throughout the surveys. Approximately 10 m outside of the test site area were measured in

261   addition to the areas inside the test sites.

262

263   *2.3. Monte Carlo Simulations*

264   The individual instruments were calibrated using Monte Carlo Simulations (MCS). MCS

265   were preferred over analytical calibration given that the relationship between PTV and

266   changes in ^{137}Cs depth distribution could be modelled with greater precision compared to a

267   limited number of soil core data (Likar et al., 2000). MCS are widely used to estimate

268   detector responses as radiation transport is probabilistic by nature and very difficult to resolve

269   use deterministic approaches (Stromswold, 1995). Hence, by tracking individual particles,

270   through repeated random sampling of well-defined probability distributions a complex

271   problem can be addressed (Maučec et al., 2009).

272

273

274

275

276

277

278

279

280

281

282

283

284

285 Table 1. Inventories, bulk soil density, soil characteristics and depth profiles of ^{137}Cs at each
286 of the five sites.
287

Soil characteristics	Layer	^{137}Cs Bq/kg	% of Total ^{137}Cs Inventory
Soddy podzolic	Site 1 0-3 cm	41450+/-8290	66.1+/-13.2
	3-6 cm	15350+/-3070	28.8+/-5.8
	6-10 cm	1360+/-270	3.6+/-0.7
	0-15 cm	314+/-72	1.1+/-0.3
	15-20 cm	92+/-27	0.3+/-0.1
	Bulk density / ^{137}Cs Inventory		1.62 g/cm^3 / 2414 kBq/m^2
Sandy	Site 2 0-3 cm	876+/-175	24.0+/-4.8
	3-6 cm	814+/-163	19.4+/-3.9
	6-10 cm	693+/-139	22.6+/-4.5
	0-15 cm	813+/-163	33.4+/-6.7
	15-20 cm	16+/-8	0.6+/-0.3
	Bulk density / ^{137}Cs Inventory		1.77 g/cm^3 / 215 kBq/m^2
Organic peat	Site 3 0-3 cm	33380+/-6675	38.7+/-7.7
	3-6 cm	16000+/-3200	30.1+/-6.0
	6-10 cm	5910+/-1180	17.3+/-3.5
	0-15 cm	2740+/-550	10.0+/-2.0
	15-20 cm	947+/-189	3.9+/-0.8
	Bulk density / ^{137}Cs Inventory		1.15 g/cm^3 / 1672 kBq/m^2
Mineral floodplain	Site 4 0-3 cm	41810+/-8360	56.6+/-11.3
	3-6 cm	8665+/-1733	22.2+/-4.4
	6-10 cm	3076+/-615	13.4+/-2.7
	0-15 cm	940+/-189	5.9+/-1.2
	15-20 cm	292+/-65	1.8+/-0.4
	Bulk density / ^{137}Cs Inventory		1.23 g/cm^3 / 1178 kBq/m^2
Ploughed mineral	Site 5 0-3 cm	2114+/-423	17.8+/-3.6
	3-6 cm	2147+/-435	15.3+/-3.1
	6-10 cm	2164+/-433	20.6+/-4.1
	0-15 cm	2235+/-447	24.9+/-5.0
	15-20 cm	1814+/-362	21.5+/-4.3
	Bulk density / ^{137}Cs Inventory		1.55 g/cm^3 / 644 kBq/m^2

288 The software package Monte Carlo N-Particle 5 (MCNP5) was used to obtain spectral

289 responses to recover PTV (Briesmeister, 1993). In individual MCS, a basic geometry

290 encompassing the detector, soil column and air filled with constituent materials were

291 described through input cards (Figure 3).

292

293 …………………………Insertion Point for Figure 3…………………………………..

294

295 **Figure 3. MCNP setup and method used to derive PTV from an exponential distributed**

296 **source.**

297

298 Descriptions of the starting source were also given to MCNP5, alongside F8 tally instructions

299 that captured the differential energy spectrum within the simulated detector's active volume.

300 Given that the PTV is generated using energies considerably higher than those significantly

301 affected by the photoelectric effect and backscatter (>350 keV), Beck et al. (1972) a standard

302 soil composition was used. All nuclide decay data was acquired from the National Nuclear

303 Data Centre (2013).

304

305 Validated detector geometries utilised in previous studies (Varley et al., 2015a) were used to

306 derive spectral responses for 71 (Ø) $\times$ 71 mm NaI:Tl and LaBr:Ce detectors. Varley et al.,

307 (2015a) reported good agreement between MCS and experimental benchmark results

308 collected from doped-concrete calibration pads (1 m^2). The code making up the detector

309 geometries was modelled on manufactures specification provided by Saint Gobain along with

310 receipt of detectors. Detector models encompassed the active volume, its outer canning, a

311 simplified photomultiplier tube and the PVC plastic piping used to house the detection unit

312 (Figure 3). The simulated contamination was an unbiased source of 0.662 MeV photons and

313 the geometry was truncated just above the detector where beyond this point all particles were

314 killed to maximise computer time. No specific reduction variance techniques were used such

315 as Russian roulette.

316

317 To optimise the geometry of the simulation, adjoint calculations were utilised to establish the

318 necessary limits or effective FoV of the detector to the source (Varley et al., 2015b). A

319 conservative extent for the surface layer (0-0.01 m) was adopted (25 m) and successively

320 deeper layers were established in the same manner. A Gaussian function was fitted to the

321 adjoint results that included 99.9 % of the total photons. Importantly, MNCP5 does not take

322 into consideration pile-up effects in the electronics of the scintillator for instance when chance

323 coincidence is encountered (Lindstrom and Fleming, 1995). This phenomenon within

324 environmental spectra can significantly alter the shape of the spectrum at high count rates

325 leading to a smearing of the spectrum and importantly removing counts from the full energy

326 peak to a higher energy channel when combined with lower energy photons (Mowlavi and

327 Hadizadeh Yazdi, 2011). Pile-up can be modelled using a Monte Carlo regime if the spectrum

328 is accurate enough across all energies. However, it was accepted that the lower energy part of

329 the spectrum could not be modelled accurately due to uncertainties associated with the

330 photoelectric effect which is driven by the chemical composition of the soil. Therefore no

331 attempt was made to model this occurrence through Monte Carlo methods. Yet, full energy

332 photon losses in the field were not expected to exceed 0.5 % even at the highest count rates

333 observed. This was established by monitoring the smearing of photons to higher energies.

334

335 To achieve spectral responses to a variety of depth distributions and inventories, MCS were

336 simulated at discrete 10 mm depth intervals down to a depth of 70 g cm^{-2} (Figure 3). Beyond

337 70 g cm^{-2} it was found that contributions to PTV were infinitesimal even for large β values.

338 To form the spectral response for a given value of β and inventory, spectral contributions

339 from each 10 mm slice were weighted in accordance with the appropriate exponential

340 function value (see Eqn [1]). This approach not only permitted the PTV to be defined at a

341 higher depth resolution but also improved counting statistics for later regression models. The

342 reason for this is that the maximum number of particles in MCNP5 (2×10^{9}) could be run in

343 each simulation effectively increasing source density without repeated random number

344 sampling (Briesmeister, 1993).

345

346 Environmental spectra obtained from the test sites contained contributions from the natural

347 radioelements: ^{40}K and the ^{238}U and ^{232}Th series. Although spectral inputs from the natural

348 nuclides were small in comparison to ^{137}Cs, contributions to the valley region were found to

349 influence the PTV particularly at low ^{137}Cs photon fluxes. Therefore, straightforward uniform

350 distributions for the natural radioelements were included as separate MCS (Thummerer and

351 Jacob, 1998).

352

353

354

2.4. Vertical Distribution of ^{137}Cs

356   In the first decade or so following Chernobyl, many early studies that used field gamma-ray

357   spectrometry to measure ^{137}Cs at undisturbed sites tended to a adopt an exponential function,

358   whereby the activity of contamination was assumed to decrease exponentially with increasing

359   depth as the heavily concentrated ^{137}Cs source on the surface gradually penetrated into the soil

360   column (Hillmann et al., 1996). A number of studies have confirmed this in Belarus and

361   PSRER (Askbrant et al., 1996; Ivanov et al., 1997) However, more recent observations from

362   other areas of Europe have shown the exponential function to break down as the source

363   further penetrates into the soil column and fresh relatively uncontaminated soil buries

364   contamination to form a subsurface maximum (Almgren and Isaksson, 2006; Bernhardsson et

365   al., 2015). However, the most recent study conducted in the PSRER suggests that the

366   exponential function is perhaps still the most appropriate (Dowdall et al., 2017). There reason

367   are three reasons that might explain this outcome. Firstly, the PSRER in comparison to other

368   parts of Europe, where many of the aforementioned studies were conducted, receives

369   relatively low annual rainfall possibly limiting penetration. Secondly, the primary mode of

370   contamination deposition at the time of the accident was dry deposition rather than wet

371   deposition reducing initial infiltration (Drozdovitch et al., 2013). Finally, within a 30 km

372   radius of the ChNPP, radiocaesium was thought to be highly associated with fuel fragments

373   significantly affecting its physiochemical form and ultimately its mobility (Smith and

374   Beresford, 2002).

375

376   These facts combined with the knowledge that the PSRER has not been disturbed to any great

377   extent in over 30 years, therefore justify an exponential decay function to be used in the

378   modelling of the ^{137}Cs depth distribution in this environment (ICRU, 1994). Wherein the

379   activity (A_m) (Bq kg^{-1}) of the soil changes with mass per unit area (ζ) (g cm^{-2}) (Eqn [1]).

380

381   $$A_m (\zeta) = A_{m,0} \cdot e^{(-\zeta/\beta)} \hspace{3cm} [1]$$

382

383   Notice, mass per unit area is preferred over physical depth (cm) as it takes into account

384   density (ρ), which generates a better approximation of shielding and thus permits inventory

385   (Bq m^{-2}) to be calculated more accurately (Eqn [1]). The relaxation mass per unit area (β)

386   relates the rate at which the surface activity (A_0) decreases with mass depth. Resultantly, β

387   values approaching 0 will define surface contamination whilst uniform contamination will

388   approach ∞.

389

390   *2.5. Peak and Valley Calculation*

391   The first step in calculation of the PTV was identification of a peak within the correct area of

392   a spectrum obtained in the field. The gain stabilisation software, in the vast majority of cases,

393   centred the 662 keV peak in the correct channel, however small amounts of spectral drift

394   occurred during the survey. To ensure the peak (NaI:Tl = 586.8-737.2 keV; LaBr:Ce = 618.3-

395   705.7 keV), valley (NaI:Tl = 496.5-583.8 keV; LaBr:Ce = 498.7-615.3 keV) and background

396   (NaI:Tl = 740.2-755.3 ; LaBr:Ce = 708.7-726.8 keV) region of interests remained the same

397   between spectra, a Gaussian function was fitted to the peak, the maximum of which could

398   then act as a more precise energy calibration. Thereafter, the background under the peak was

399   estimating using a straightforward linear model fitted to five channels either side of the base

400   of the peak. The background was then subtracted and a second Gaussian function was fitted

401   and integrated to calculate the area. The valley height was calculated by subtracting the area

402   to the high energy side of the peak from the valley region (Tyler, 2004). This routine was

403   written using the base features of the R statistical package (R Core Development Team,

404   2016).

405

406   *2.6. Data Generation*

407   For each detector a calibration dataset was generated, comprised of 1000 spectral responses,

408   derived through randomly sampling input β and inventory parameters and applying them to

409   the MCS dataset. The calibration dataset provided spectra with relatively low uncertainty to

410   facilitate fitting of statistical models. An independent dataset (of 2000 spectral responses) was

411   also formed. This dataset, known as the cross-validation dataset, provided a means of

412   assessing performance through Root Mean Square Error (RMSE) for β and inventory

413   estimates. The same modelling constraints applied to the calibration dataset were used to form

414   the cross-validation dataset, but with the addition of the natural radionuclides ([40]K, [238]U and

415   [232]Th series) and Poisson noise generated from the one second counts. A similar

416   bootstrapping subroutine of MCS has proven valuable in previous studies to sample both

417   background and source populations when *a priori* knowledge is not available (Varley et al.,

418   2015b).

419

420 Model parameters (Table 2) were chosen to be representative of the variation that could take

421 place within the PSRER environment. Simulated inventories were markedly higher than

422 those at the five test sites, but it was deemed necessary to develop an approach that could be

423 used for higher deposition densities. Additionally, a maximum β value of 100 was chosen as

424 it was discovered through preliminary investigations that larger values contributed negligible

425 counts into the valley regions and would be almost impossible to differentiate. In any case, β

426 values above 100 make very little difference to final inventory estimations and will have

427 negligible contribution if dose rate calculations are performed (ICRU, 1994).

428

429

430 Table 2. Parameters used to construct a synthetic dataset.

Parameter	Minimum	Mean	Median	Maximum
^{137}Cs inventory (kBq m^{-2})	7.2	2479.3	282	86962.2
β (g cm^{-2})	0.13	18.3	7.6	100.0
^{40}K inventory (kBq m^{-2})	28.2	226.7	222.6	565.2
^{238}U inventory (kBq m^{-2})	7.1	17.5	16.7	42.39
^{232}Th inventory (kBq m^{-2})	7.1	19.3	18.4	42.4

431

432 *2.7. Calibration Curves*

433 To establish appropriate calibration curves to estimate β and inventory for each detector, a

434 linear model was fitted to the respective calibration datasets through a conventional least-

435 squares fitting regime (Crawley, 2012). The relationship between explanatory and response

436 variables was found to be log-linear whereby both response (β) and explanatory (PTV)

437 variables were logarithmic. Formulation of the depth model was performed by regressing

438 PTV against β, where β_0 is the point at which PTV is equal to zero and βs is the slope factor

439 applied to PTV (Eqn [1])

440

441 $$log(\beta) = \beta_0 + \beta_s \cdot log(PTV) \hspace{3cm} [2]$$

442

443   The inventory model was estimated by calculating the calibration coefficient C, by dividing

444   the inventory *(A)* by the number of counts in the full energy peak *(N_p)* (Eqn [3]). *C* could then

445   be regressed against the PTV to generate the intercept (C_0) and the slope factor (C_s) (Eqn [4]).

446

447
$$C = A/N_p \qquad\qquad\qquad [3]$$

448

449
$$log(C) = C_0 + C_s \cdot (PTV) \qquad\qquad [4]$$

450

451   Applied to field estimates the PTV can be used to derive C, which need only be multiplied by

452   N_p to estimate inventory (Tyler et al., 1996b).

453

454   *2.8. Detector-core Comparisons*

455   To develop a firm basis for statistical comparison with the soil core results, all spectra

456   obtained inside the sites were isolated using a georeferenced polygon, run through the

457   calibrated models and then aggregated to form a median and interquartile ranges. On average

458   approximately 600 spectra were collected at each site. Median and interquartile ranges were

459   preferred over the mean and standard deviation as estimates were found to be highly skewed.

460   Core inventory estimates were the sum of the total activity of the core multiplied by the

461   reciprocal of the total core diameter (m^2). Uncertainties were principally based on counting

462   uncertainty. Derivation of β for core data was performed by using a least-squares fitting

463   regime on the function described in Eqn [1]. Uncertainties were derived by Monte Carlo

464   simulation.

465

3. Results and Discussion

3.1. Statistical Modelling of Monte Carlo Simulations

Statistically significant relationships (R^2 values greater than 0.93; $p < 0.05$) were found for all models derived from the calibration datasets (Table 3). Model parameter values are similar between detectors, suggesting that the detectors respond in a similar manner to an extended environmental ^{137}Cs source.

Table 3. Parameter and R^2 values for depth and inventory models for lanthanum bromide and sodium iodide detectors.

| Detector | B_0 | Depth model | | | | Inventory model | | | |
		B_s	R^2	$RMSE$	C_0	C_s	R^2	$RMSE$
LaBr:Ce	1579.71	0.97	0.93	19.32	10.23	0.98	0.98	407.21
NaI:Tl	1423.46	0.97	0.94	22.04	11.92	0.98	0.99	483.85

Based on RMSE values on validation datasets in which Poisson noise and natural background were introduced, LaBr:Ce (407.21 kBq m^{-2} and 19.32 g cm^{-2}) marginally outperformed NaI:Tl (483.85 kBq m^{-2} and 22.04 g cm^{-2}) (Table 3). LaBr:Ce would at this stage appear to offer increased performance. Nonetheless, to investigate the response of each detector further the average uncertainty made on inventory and β estimates, as a function inventory, has been presented (Figure 4).

................................*Insertion Point for Figure 4*..

Figure 4. A) Percentage error associated with inventory estimates as a function of inventory for: lanthanum bromide (purely based on peak counts), lanthanum bromide (peak-to-valley corrected) and sodium iodide (peak-to-valley corrected) B) Percentage error associated with β estimates as a function of inventory for lanthanum bromide (peak-to-valley corrected) and sodium iodide (peak-to-valley corrected).

491

492 Firstly, the advantage of using PTV corrected data can be realised when compared to

493 uncorrected data derived from peak counts (Figure 4A). At inventories greater than 100 kBq

494 m^{-2}, there is clear divergence in the percentage error on inventory estimates between corrected

495 and uncorrected LaBr:Ce results, which becomes significantly larger as inventory increases.

496 This occurrence can be explained through counting statistics. For example, at low peak count

497 rates (typically of the order of a few hundred) the uncertainty associated with the calculation

498 of PTV is large enough that it does not aid in the estimation of inventory; the highest source

499 of uncertainty in this instance will be associated with the valley height calculation. However,

500 as count rates rise with increasing contamination, and the valley calculation becomes more

501 reliable, the PTV correction significantly decreases the percentage error associated with

502 inventory estimation.

503

504 Reinforcing the RMSE values (Table 3), corrected NaI:Tl and LaBr:Ce would appear to

505 produce similar percentage error across the inventory range (Figure 4A). Yet, at inventories

506 less than ~1500 kBq m^{-2}, NaI:Tl exhibits an advantage of ca. 5% lower percentage error than

507 LaBr:Ce. Above ~1500 kBq m^{-2}, LaBr:Ce would appear to improve on NaI:Tl by

508 approximately 1%. This fact is associated with the intrinsic background contained with the

509 LaBr:Ce active volume. Therefore, at lower count rates, the signal to noise ratio is lower than

510 that of NaI:Tl, nonetheless, when count rates exceed a roughly thousand or more the

511 improved energy resolution deems it superior. A similar aspect is observed when analysing

512 percentage error associated with β estimates as a function of inventory (Figure 4B). Note,

513 there is a similar crossover at approximately ~1000 kBq m^{-2}, but in this case the advantage

514 above this value is clearer for the LaBr:Ce detector (~10%). Interestingly, percentage error

515 on β values are seen to plateau for both detectors at densities around 4000 kBq m^{-2}. This

516 possibly represents the absolute limit of detection where very little improvement on depth

517 estimate can be made using the devices, this is due to the sensitivity of the ratio at greater

518 values of β.

519

520 *3.2. Application to the Reference Sites*

521 Core results confirmed that there was a large variation in both the depth distribution and total

522 inventory across the five test sites (Figure 5). General patterns included a clear surface

523 association of contamination at the high activity organic-rich sites (1, 3 and 4) and sites with

524   significant vertical penetration: sites 2 (sandy) and 5 (ploughed). Applying the models

525   developed from MCS to data collected over the test sites yielded encouraging results.

526   Generally, there was good agreement between core and detector inventory estimates

527   particularly for sites 1, 2 and 4 with less than 25 % difference between core and detector

528   estimates (Figure 6A).

529

530   ……………………………....*Insertion Point for Figure 5*……………………………………

531

532   ***Figure 5. Inventory depth distributions derived from soil cores extracted from the five***

533   ***GAMFAC sites. Uncertainties are one standard deviation and based on counting statistics.***

534

535   Results are very similar for both detectors for all of the sites confirming earlier percentage

536   error investigations (see Figure 4A). The detectors struggled equally to characterise the

537   inventory at sites 2 and 5 where differences of ca. 53 % and 45 % were encountered (see

538   Figure 6A). It became clear that this method may be limited at sites were the level of

539   contamination is relatively low and at greater depths when operating with one second count

540   times. To lower the uncertainty, it might be appropriate to lengthen the count time or,

541   alternatively, conduct slower traverses and increasing the spatial density of spectra, which

542   could, retrospectively, be summed to improve statistics. It must also be noted that remote

543   measurements tend to only sample the top 20 cm or so of soil, much of the contamination at

544   these sites is below this range and most possibly beyond the detection capabilities of these

545   instruments (see Figure 4A). In addition, it may be argued that these sites could be described

546   as a having subsurface maxima ($\sim$20 g cm^{-2}), which the exponential model would have

547   struggled to accurately characterise (see Figure 5). Alternate more flexible models, for

548   example the one described by Hillman et al. (1996) or (Almgren and Isaksson, 2006) might be

549   more appropriate in this case. This could have been more representative of the PTV values

550   found in the field and reduced the uncertainty associated with final inventory estimates.

551

552   …………………………….... *Insertion Point for Figure 6* ………………………….

553

554   ***Figure 6. Median and interquartile range values for inventory (A) and β (B) estimates for***

555   ***the five GAMFAC sites for lanthanum bromide and sodium iodide compared to core***

556   ***results.***

557 An example of how complex the spatial distribution of ^{137}Cs in the PSRER can be is
558 provided, whereby inventory and β values obtained using NaI:Tl from site 2 and the area
559 surrounding have been smoothed using universal kriging (Graphical abstract). First of all,
560 notice the reference site chosen on the sand dune (red broken lines) was relatively stable with
561 little variation in inventory and depth confirming it a good choice of reference site to apply
562 static *in situ* systems. However, outside of the isolated site large fluctuations in inventory and
563 depth were witnessed. For instance two relatively large hotspots (5-15 meters in diameter) to
564 the north of the site were estimated to possess more than six times the inventory (~1500 kBq
565 m^{-2}) of the reference site. Due to the geometry and distance away from the reference site
566 these sources would nonetheless have little impact on final calibration measurements taken at
567 the site. Together with greater inventory, β values associated with these hotspot were
568 estimated to be greater than the surrounding area suggesting contamination was deeper in the
569 soil column. This finding could suggest accumulation and penetration of contamination
570 particularly in areas of the topographic depression in the foreground, which was lower in
571 elevation than the sand dune and could potentially accumulate ^{137}Cs through erosion
572 processes. Further investigative studies involving coring and chemical analysis would have to
573 be performed to confirm this hypothesis.
574
575 *Graphical abstract. Estimated inventory and β obtained for 71 × 71 mm sodium iodide*
576 *detector for site 2 (red box) and surrounding area. Notice the reference site (red box) is*
577 *significantly more stable than surrounding areas in terms of depth and activity.*

4. Conclusions

The Chernobyl Nuclear power plant disaster has been the single largest nuclear reactor meltdown in our history. Subsequently, highly radioactive material can be found in large areas of Ukraine, Belarus and Russia presenting a considerable remediation challenge that could take decades or even centuries to overcome. An important step in this process is develop methods to characterise the activity and burial depth of ^{137}Cs in high spatial resolution. To this end, a highly practical method has been described and validated against reference sites within the Polessie State Radioecological Reserve in southern Belarus. It was shown that a conventional 71×71 mm sodium iodide scintillation detector could exhibit equal performance to a significantly more expensive lanthanum bromide detector of the same size and power requirements. This outcome can be attributed to the intrinsic contamination associated with lanthanum bromide. Depth and activity maps of ^{137}Cs contamination have demonstrated the advantage of the technique applied to the sodium iodide detector. Further application of this approach could significantly support future remediation activities ultimately lowering the risk to human health.

5. Acknowledgements

627 **References**

628

629 Almgren, S., Isaksson, M., 2006. Vertical migration studies of ^{137}Cs from nuclear weapons
630   fallout and the Chernobyl accident. J. Environ. Radioact. 91, 90–102.
631   doi:10.1016/j.jenvrad.2006.08.008

632 Askbrant, S., Melin, J., Sandalls, J., Rauret, G., Vallejo, R., Hinton, T., Cremers, A.,
633   Vandecastelle, C., Lewyckyj, N., Ivanov, Y.A., Firsakova, S.K., Arkhipov, N.P.,
634   Alexakhin, R.M., 1996. Mobility of radionuclides in undisturbed and cultivated soils in
635   Ukraine, Belarus and Russia six years after the Chernobyl fallout. J. Environ. Radioact.
636   31, 287–312. doi:10.1016/0265-931X(95)00054-E

637 Beck, H., DeCampo, J., Gogolak, C., 1972. In situ Ge(Li) and NaI(Tl) gamma-ray
638   spectrometry. New York. doi:10.2172/4599415

639 Bernhardsson, C., Roof, C.L., Mattsson, S., 2015. Spatial variability of the dose rate from
640   137Cs fallout in settlements in Russia and Belarus more than two decades after the
641   Chernobyl accident. J. Environ. Radioact. 149, 144–149.
642   doi:http://dx.doi.org.ezproxy.stir.ac.uk/10.1016/j.jenvrad.2015.07.009

643 Briesmeister, J.F., 1993. MCNP-A general Monte Carlo N-particle transport code. LA-12625.

644 Center, N.N.D., 2013. Nuclear datasheets. URL http://www.nndc.bnl.gov/ensdf/

645 Crawley, M.J., 2012. The R book. John Wiley & Sons. ISBN-13: 978-0470510247

646

647 Dowdall, M., Bondar, Y., Skipperud, L., Zabrotski, V., Pettersen, M.N., Selnæs, G., Brown,
648   J.E., 2017. Investigation of the vertical distribution and speciation of ^{137}Cs in soil
649   profiles at burnt and unburnt forest sites in the Belarusian Exclusion Zone. J. Environ.
650   Radioact. 175-176, 60–69. doi:10.1016/j.jenvrad.2017.04.009

651 Dowdall, M., Bondar, Y.I., Fristrup, P., Guonason, K., Granstrom, M., Hedman, A., Israelson,
652   C., Jonsson, G., Kjerulf, S., Juul Krogh, S., Mauring, A., Moller, B., Tyler, A.N., Varley,
653   A., Zabrotski, V., 2015. Advanced In-situ Gamma Spectrometry Field Activity
654   Chernobyl (GAMFAC), GAMFAC. Nordic Nuclear Safety Research, Denmark.

655 Drozdovitch, V., Zhukova, O., Germenchuk, M., Khrutchinsky, A., Kukhta, T., Luckyanov,

656 N., Minenko, V., Podgaiskaya, M., Savkin, M., Vakulovsky, S., Voillequ�, P., Bouville,

657 A.A., Voillequé, P., Bouville, A.A., 2013. Database of meteorological and radiation

658 measurements made in Belarus during the first three months following the Chernobyl

659 accident. J. Environ. Radioact. 116, 84–92.

660 doi:http://dx.doi.org.ezproxy.stir.ac.uk/10.1016/j.jenvrad.2012.09.010

661 Duval, M., Arnold, L.J., 2013. Field gamma dose-rate assessment in natural sedimentary

662 contexts using LaBr3(Ce) and NaI(Tl) probes: A comparison between the "threshold"

663 and "windows" techniques. Appl. Radiat. Isot. 74, 36–45.

664 doi:10.1016/j.apradiso.2012.12.006

665 Feng, T.C., Jia, M.Y., Feng, Y.J., 2012. Method-sensitivity of in-situ gamma spectrometry to

666 determine the depth-distribution of anthropogenic radionuclides in soil. Nucl.

667 Instruments Methods Phys. Res. Sect. A-Accelerators Spectrometers Detect. Assoc.

668 Equip. 661, 26–30. doi:10.1016/j.nima.2011.09.014

669 Gering, F., Hillmann, U., Jacob, P., Fehrenbacher, G., 1998. In situ gamma-spectrometry

670 several years after deposition of radiocesium II. Peak-to-valley method. Radiat. Environ.

671 Biophys. 37, 283–291. doi:10.1007/s004110050130

672 Gering, F., Kiefer, P., Fesenko, S., Voigt, G., 2002. In situ gamma-ray spectrometry in

673 forests: determination of kerma rate in air from [137]Cs. J. Environ. Radioact. 61, 75–89.

674 doi:http://dx.doi.org/10.1016/S0265-931X(01)00116-3

675 Guermentchuk, M.G., Zhukova, O.M., Shagalova, E.D., Matveenko,, I.I. 1997.

676 Radioecological mapping of the territory of Belarus on the base information of radiation

677 monitoring. In: IAEA-TECDOC-980. Uranium Exploration Data and Techniques

678 Applied to the Preparation of Radioelement Maps, Proceedings of a Technical

679 Committee Meeting, International Atomic Energy Agency (IAEA), Vienna. ISSN

680 1011-4289. Pp. 153-161

681

682 Guss, P., Reed, M., Yuan, D., Cutler, M., Contreras, C., Beller, D., 2010. Comparison of

683 CeBr(3) with LaBr(3):Ce, LaCl(3):Ce, and NaI:Tl Detectors. Proc. SPIE-The Int. Soc.

684 Opt. Eng. 7805, 78050L–78050L. doi:10.1117/12.862579

685 Hillmann, U., Schimmack, W., Jacob, P., Bunzl, K., 1996. In situ gamma-spectrometry

686   several years after deposition of radiocesium .1. Approximation of depth distributions by
687   the Lorentz function. Radiat. Environ. Biophys. 35, 297–303.
688   doi:10.1007/s004110050043

689 International Commission on Radiation Units (ICRU), 1994. Gamm-Ray Spectrometry in the
690   Environmental. International Commission on the Radiation Units and Measurements,
691   7910 Woodmont Avenue Bethesda, Maryland 20814, U.S.A.

692 Iltis, A., Mayhugh, M.R., Menge, P., Rozsa, C.M., Selles, O., Solovyev, V., 2006. Lanthanum
693   halide scintillators: Properties and applications. TRDs Third Millenium Proc. 3rd Work.
694   Adv. Transit. Radiat. Detect. Accel. Sp. Appl. 3rd Work. Adv. Transit. Detect. Accel.
695   Sp. Appl. 563, 359–363. doi:10.1016/j.nima.2006.02.192

696 Izrael, Yu.A., Bogdevich, I.M. (Eds.) 2009. The Atlas of recent and predictable aspects of
697   consequences of Chernobyl accident on polluted territories of Russia and Belarus
698   (ARPA Russia-Belarus) Moscow-Minsk: Infosphere Foundation NIA-Nature.
699

700 Ivanov, Y.A., Lewyckyj, N., Levchuk, S.E., Prister, B.S., Firsakova, S.K., Arkhipov, N.P.,
701   Arkhipov, A.N., Kruglov, S. V., Alexakhin, R.M., Sandalls, J., Askbrant, S., 1997.
702   Migration of 137Cs and 90Sr from Chernobyl fallout in Ukrainian, Belarussian and
703   Russian soils. J. Environ. Radioact. 35, 1–21. doi:10.1016/S0265-931X(96)00036-7

704 Kastlander, J., Bargholtz, C., 2005. Efficient in situ method to determine radionuclide
705   concentration in soil. Nucl. Instruments Methods Phys. Res. Sect. A-Accelerators
706   Spectrometers Detect. Assoc. Equip. 547, 400–410. doi:10.1016/j.nima.2005.03.143

707 Knatko, V.A., Skomorokhov, A.G., Asimova, V.D., Strakh, L.I., Mironov, V.P. 1996.
708   Characteristics of ^{90}Sr, ^{137}Cs and $^{239,\,240}$Pu migration in undisturbed soils of southern
709   Belarus after the Chernobyl accident. J. Environ. Radioact, 30(2): 185-196,
710   http://dx.doi.org/10.1016/0265-931X(95)00011-X
711

712 Knoll, G.F., 2010. Radiation detection and measurement. John Wiley & Sons. ISBN : 978-1-
713   118-02691-5

714   Kudelsky, A.V., Smith, J.T., Ovsiannikova, S.V., Hilton, J. 1996. Mobility of Chernobyl-

715   derived ^{137}Cs in a peatbog system within the catchment of the Pripyat River, Belarus. Sci.

716   Total Environ. 188(2–3), 101-113, http://dx.doi.org/10.1016/0048-9697(96)05162-5

717

718   Likar, A., Omahen, G., Vidmar, T., Martincic, R., 2000. Method to determine the depth of Cs-

719   137 in soil from in-situ gamma-ray spectrometry. J. Phys. D. Appl. Phys. 33, 2825.

720   http://stacks.iop.org/0022-3727/33/i=21/a=323

721   Lindstrom, R., Fleming, R., 1995. Dead time, pileup, and accurate gamma-ray spectrometry.

722   Radioact. Radiochem. 6, 20–27.

723   Maučec, M., Hendriks, P.H.G.M., Limburg, J., de Meijer, R.J., 2009. Determination of

724   correction factors for borehole natural gamma-ray measurements by Monte Carlo

725   simulations. Nucl. Instruments Methods Phys. Res. Sect. A Accel. Spectrometers,

726   Detect. Assoc. Equip. 609, 194–204. doi:http://dx.doi.org/10.1016/j.nima.2009.08.054

727   Milbrath, B.D., Choate, B.J., Fast, J.E., Hensley, W.K., Kouzes, R.T., Schweppe, J.E., 2007.

728   Comparison of LaBr3:Ce and NAI(Tl) scintillators for radio-isotope identification

729   devices. Nucl. Instruments Methods Phys. Res. Sect. A Accel. Spectrometers, Detect.

730   Assoc. Equip. 572, 774–784. doi:10.1016/j.nima.2006.12.003

731   Miller, M.L., 2007. Cesium-137 in the Environment: Radioecology and Approaches to

732   Assessment and Management. NCRP Rep. No.154, Cesium-137 Environ. Radioecol.

733   Approaches to Assess. Manag. 151. ISBN-10: 0-929600-91-6

734   Mowlavi, A.A., Hadizadeh Yazdi, M.H., 2011. Monte Carlo simulation of pulse pile-up effect

735   in gamma spectrum of a PGNAA system. Nucl. Instruments Methods Phys. Res. Sect. A

736   Accel. Spectrometers, Detect. Assoc. Equip. 660, 104–107.

737   doi:10.1016/j.nima.2011.09.022

738   Nilsson, J.M.C., 2010. Using the LaBr3:Ce scintillation detector for mobile γ-spectrometry .

739   Department of Medical Radiation Physics, Lund University (Master's thesis).

740   Nilsson, J.M.C., Östlund, K., Söderberg, J., Mattsson, S., Rääf, C., 2014. Tests of HPGe- and

741   scintillation-based backpack γ-radiation survey systems. J. Environ. Radioact. 135, 54–

742   62. doi:10.1016/j.jenvrad.2014.03.013

743   ORTEC, 2005. MAESTRO (computer software)

744   Plamboeck, A.H., Nylén, T., Ågren, G., 2006. Comparative estimations of ^{137}Cs distribution
745   in a boreal forest in northern Sweden using a traditional sampling approach and a
746   portable NaI detector. J. Environ. Radioact. 90, 100–109.
747   doi:10.1016/j.jenvrad.2006.06.011

748   Povinec, P.P., Bailly du Bois, P., Kershaw, P.J., Nies, H., Scotto, P., 2003. Temporal and
749   spatial trends in the distribution of ^{137}Cs in surface waters of Northern European Seas - a
750   record of 40 years of investigations. Worldw. Mar. Radioact. Stud. 50, 2785–2801.
751   doi:http://dx.doi.org/10.1016/S0967-0645(03)00148-6

752   R Core Development Team, 2016. R: A language and environment for statistical computing.
753   R A Lang. Environ. Stat. Comput.

754   Smith, J.T., Beresford, N.A., 2002. Radioactive fallout and environmental transfers.
755   Chernobyl — Catastr. Consequences 35–80. doi:10.1007/3-540-28079-0_2

756   Sokolik, G.A., Ivanova, T.G., Leinova, S.L., Ovsiannikova, S.V., Kimlenko, I.M. 2001.
757   Migration ability of radionuclides in soil-vegetation cover of Belarus after Chernobyl
758   accident. Env. Int. , 26(3): 183-187. http://dx.doi.org/10.1016/S0160-4120(00)00104-5
759

760   Sowa, W., Martini, E., Gehrcke, K., Marschner, P., Naziry, M.J., 1989. Uncertainties of in
761   situ gamma spectrometry for environmental monitoring. Radiat. Prot. Dosimetry 27, 93–
762   101. https://doi.org/10.1093/oxfordjournals.rpd.a080450

763   Stromswold, D.C., 1995. Calibration facilites for borehole and surface environmental
764   radiation measurements. J. Radioanal. Nucl. Chem. 194, 393–401.
765   10.1007/BF02038439

766   Thummerer, S., Jacob, P., 1998. Determination of depth distributions of natural radionuclides
767   with in situ gamma-ray spectrometry. Nucl. Instruments Methods Phys. Res. Sect. A-
768   Accelerators Spectrometers Detect. Assoc. Equip. 416, 161–178. doi:10.1016/S0168-
769   9002(98)00636-6

770   Tyler, A., 2008. In situ and airborne gamma-ray spectrometry. Radioact. Environ. 11, 407-
771   448. https://doi.org/10.1016/S1569-4860(07)11013-5Tyler, A., Sanderson, D., Scott, E.,

772   1996a. Accounting for spatial variability and fields of view in environmental gamma ray

773   spectrometry. J. Environ. http://dx.doi.org/10.1016/S1569-4860(07)11013-5

774   Tyler, A., Sanderson, D., Scott, E., 1996b. Estimating and accounting for ^{137}Cs source burial

775   through in-situ gamma spectrometry in salt marsh environments. J. Environ.

776   http://dx.doi.org/10.1016/0265-931X(95)00098-U

777   Tyler, A.N., 2004. High accuracy in situ radiometric mapping. J. Environ. Radioact. 72, 195–

778   202. doi:10.1016/S0265-931X(03)00202-9

779   United Nations Scientific Committee on the Effects of Atomic Radiation (UNSCEAR), 2000.

780   Annex J: Exposures and Effects of the Chernobyl Accident. 115 p.

781

782   Varley, A., Tyler, A., Smith, L., Dale, P., 2015b. Development of a neural network approach

783   to characterise ^{226}Ra contamination at legacy sites using gamma-ray spectra taken from

784   boreholes. J. Environ. Radioact. 140, 130–140. doi:10.1016/j.jenvrad.2014.11.011

785   Varley, A., Tyler, A., Smith, L., Dale, P., Davies, M., 2015a. Remediating radium

786   contaminated legacy sites: Advances made through machine learning in routine

787   monitoring of "hot" particles. Sci. Total Environ. 521-522, 270–279.

788   doi:10.1016/j.scitotenv.2015.03.131

789   Webster, S.C., Byrne, M.E., Lance, S.L., Love, C.N., Hinton, T.G., Shamovich, D., Beasley,

790   J.C., 2016. Where the wild things are: influence of radiation on the distribution of four

791   mammalian species within the Chernobyl Exclusion Zone. Front. Ecol. Environ. 14, 185–

792   190. http://dx.doi.org/10.1002/fee.1227

793

794   Yoschenko, V.I., Kashparov, V.A., Levchuk, S.E., Glukhovskiy, A.S., Khomutinin, Y. V,

795   Protsak, V.P., Lundin, S.M., Tschiersch, J., 2006. Resuspension and redistribution of

796   radionuclides during grassland and forest fires in the Chernobyl exclusion zone: part II.

797   Modeling the transport process. J. Environ. Radioact. 87, 260–278.

798   doi:http://dx.doi.org/10.1016/j.jenvrad.2005.12.003

799   Zombori, P., Németh, I., Andrâsi, A., Lettner, H., 1992. In-situ gamma-spectrometric

800   measurement of the contamination in some selected settlements of Byelorussia (BSSR),

801   Ukraine (UkrSSR) and the Russian Federation (RSFSR). J. Environ. Radioact. 17, 97–

802   106. doi:http://dx.doi.org/10.1016/0265-931X(92)90019-P

803

804

805

806

807

808

809

810

811

812

813

814

815

816
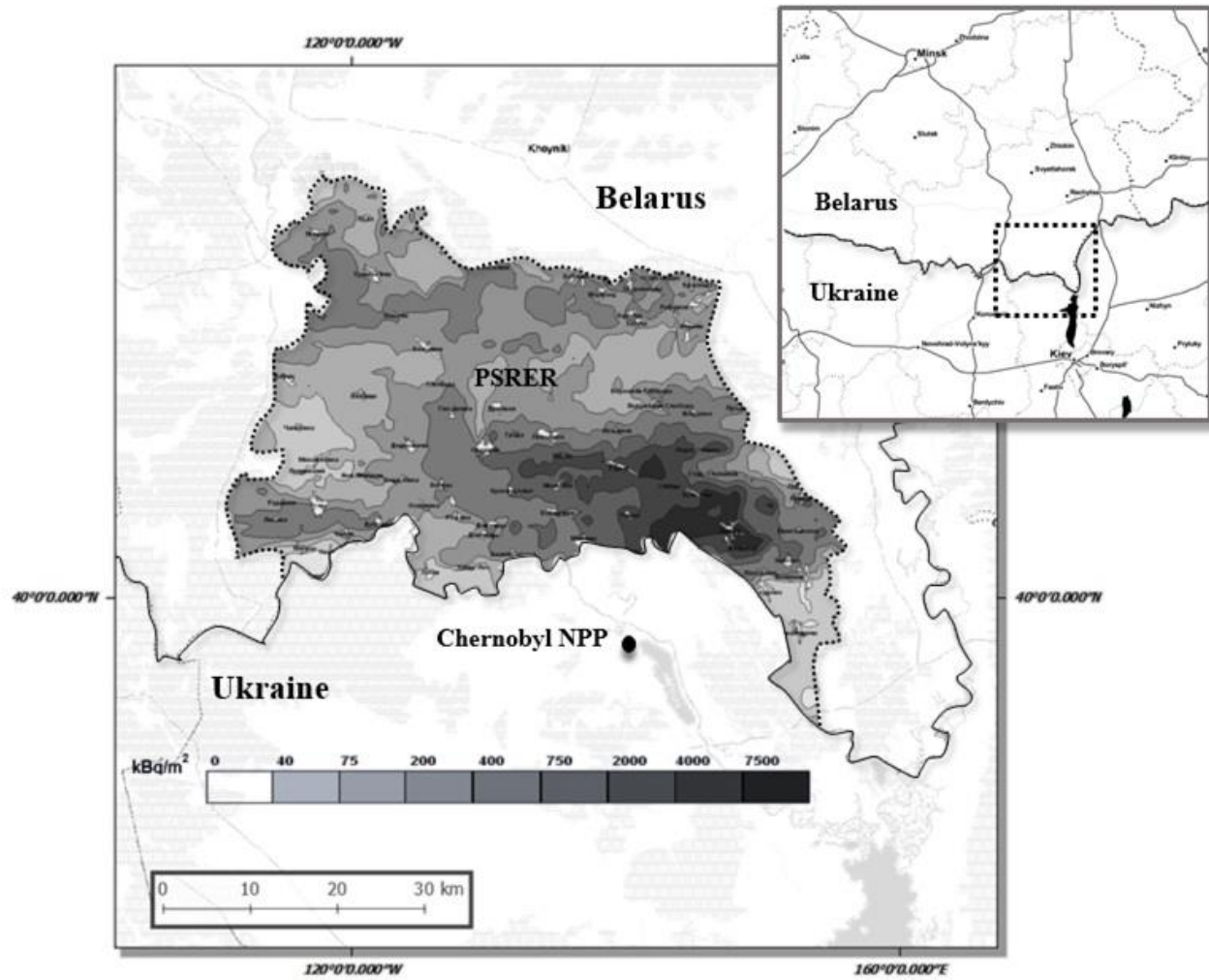
817

818

819

820

821
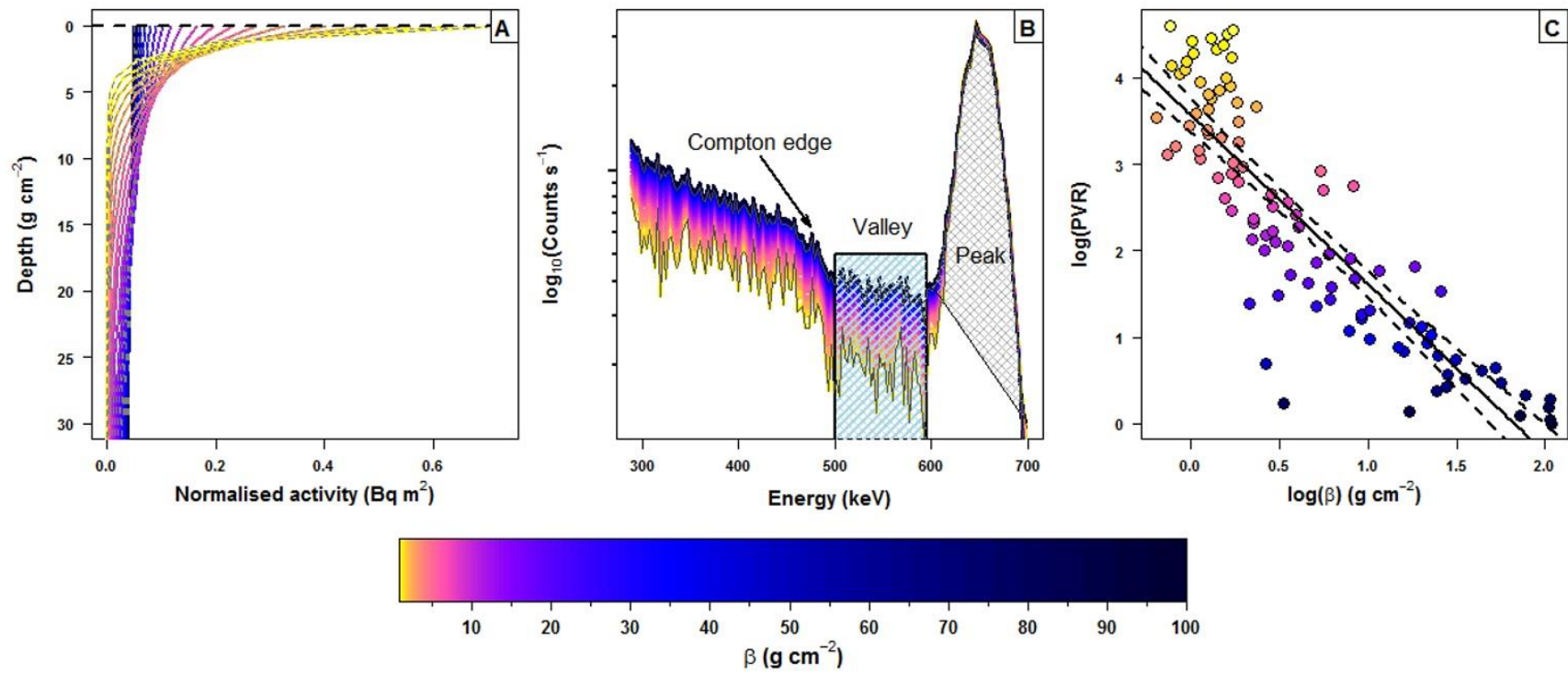
822

823

824

825

826

827

828

829

830

831
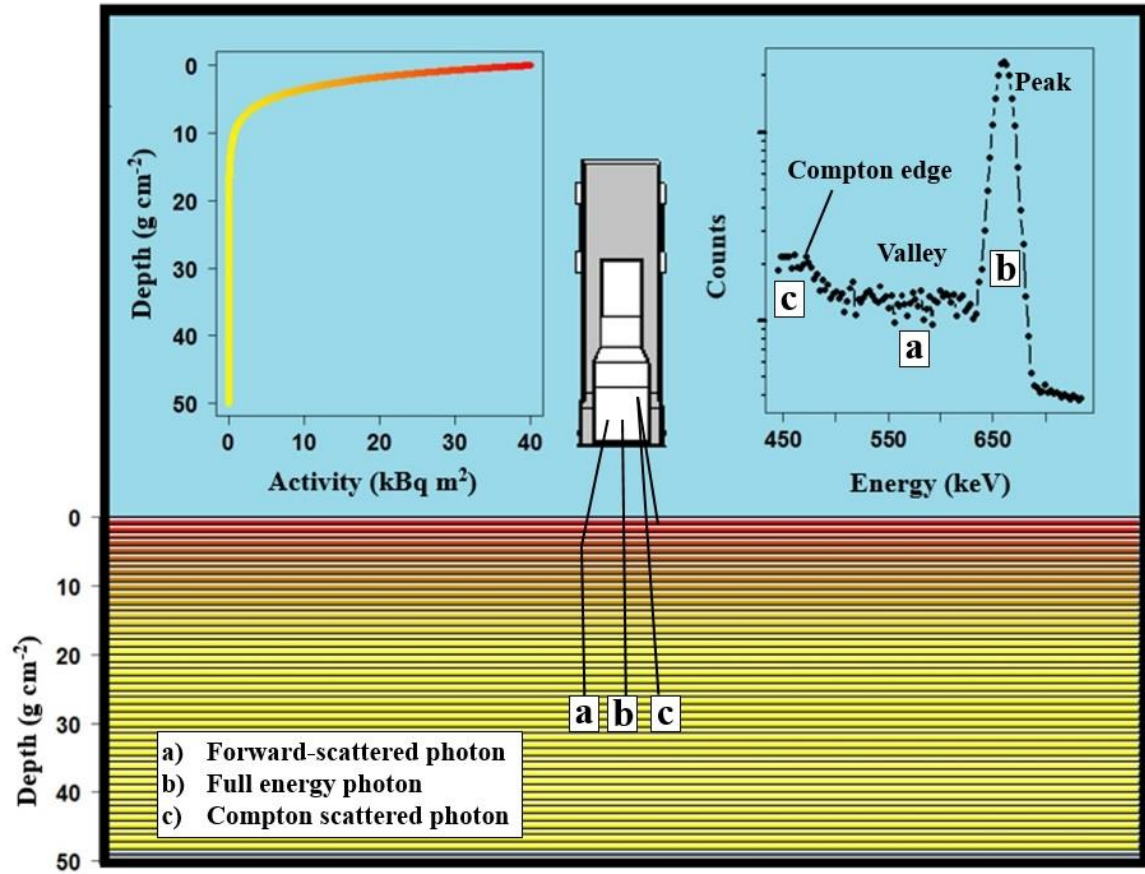
832

833

834

Figure 1
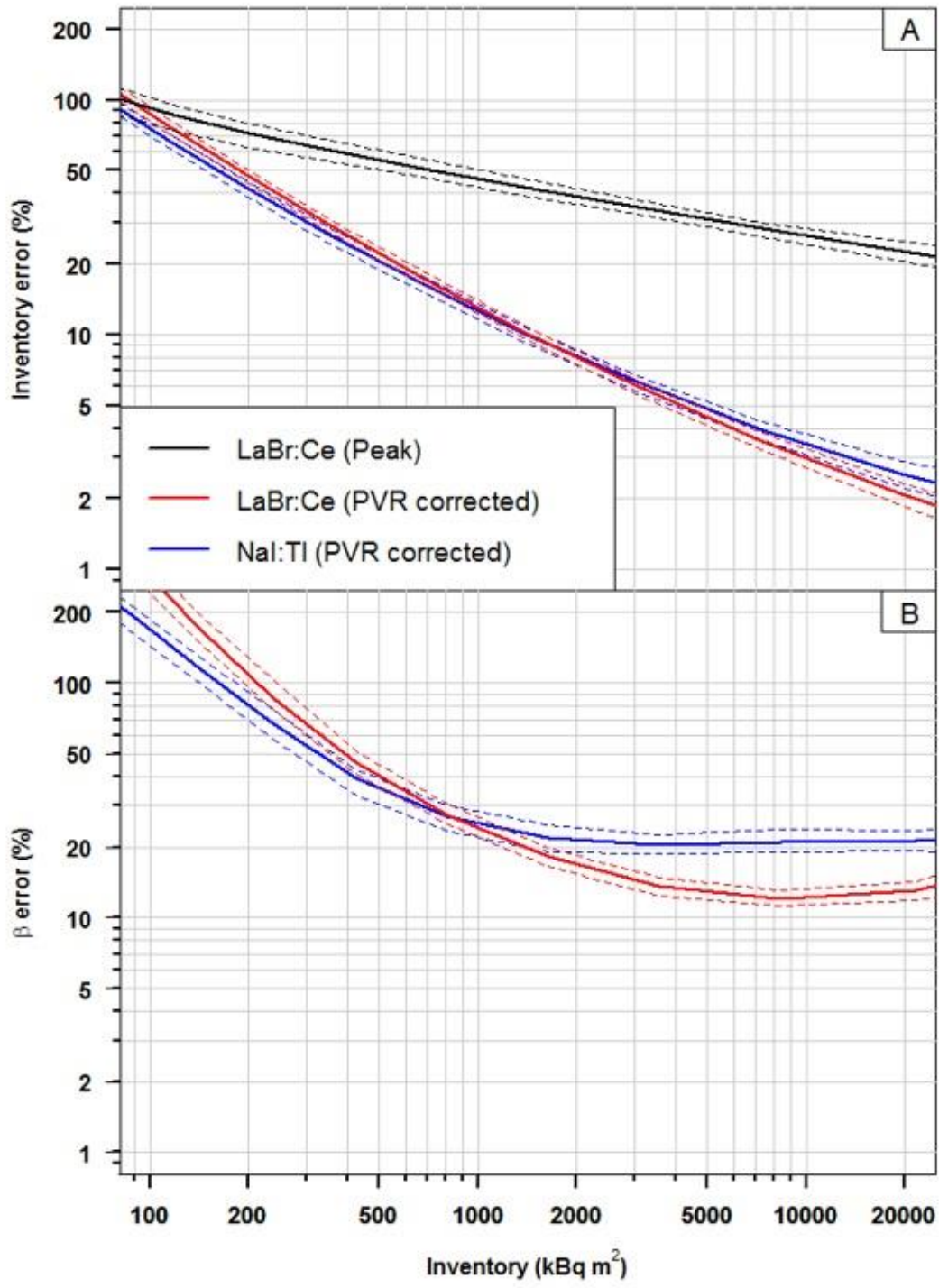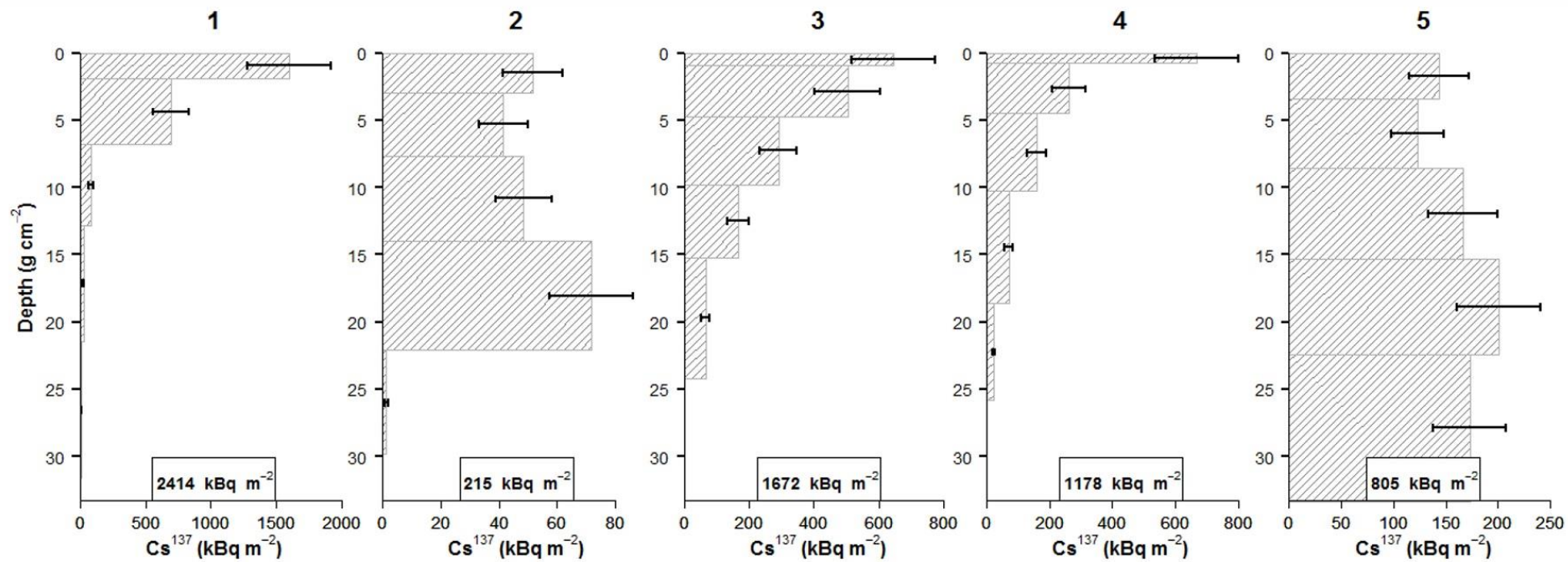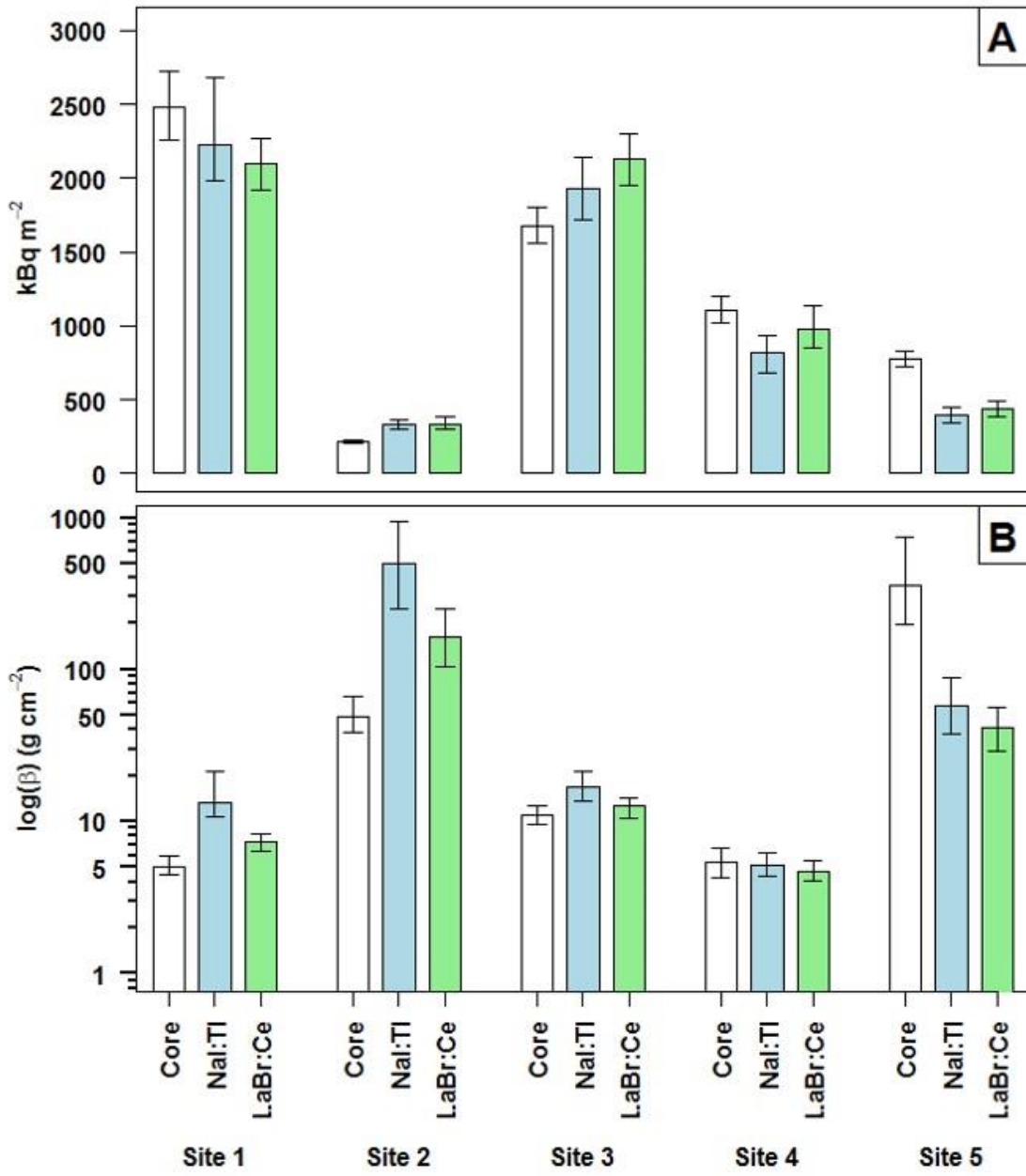
836

837

Figure 2

839

840   *Figure 3*

841

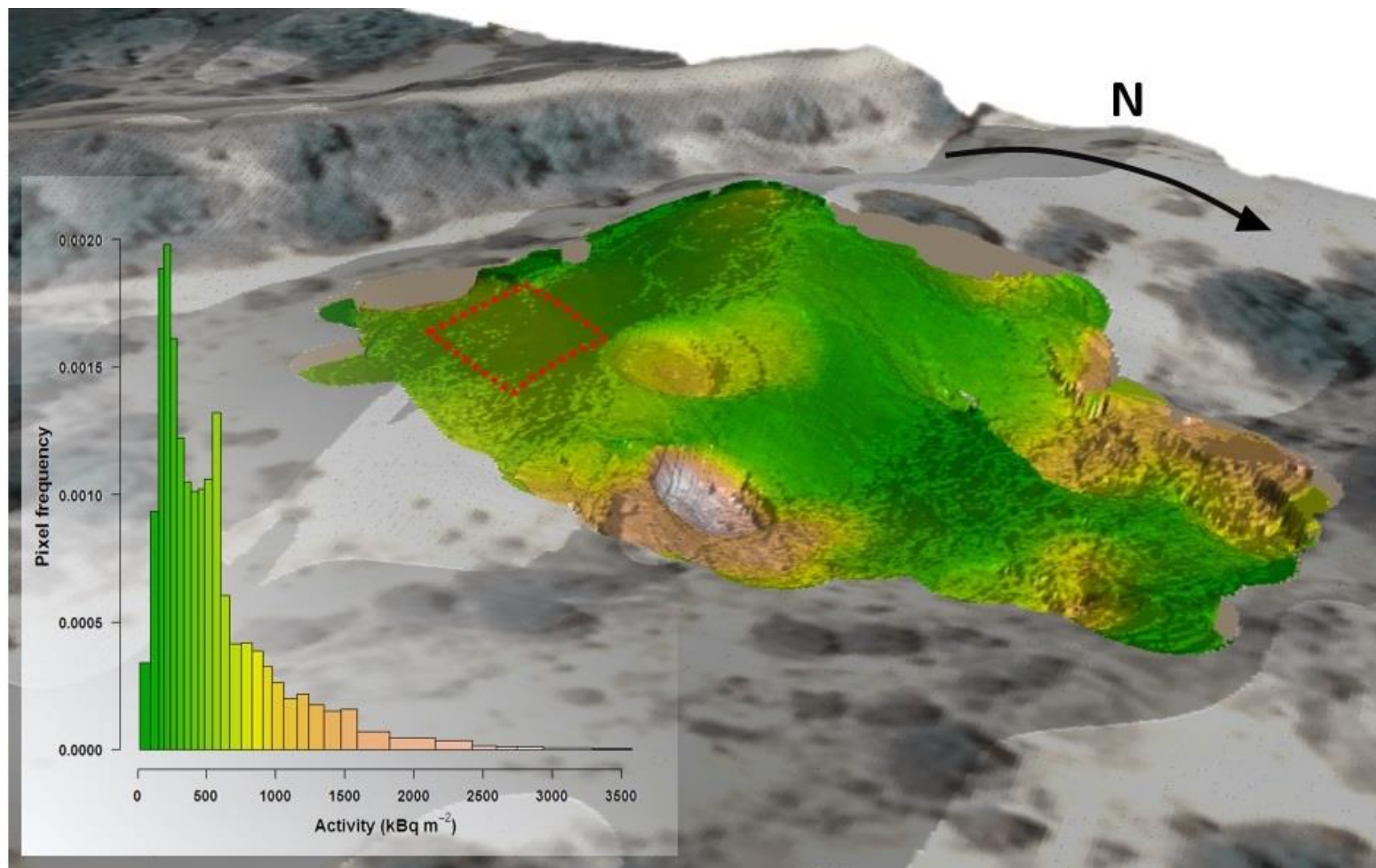842 *Figure 4*

843

844   *Figure 5*

845

846

847 *Figure 6*

848

849

850

851
852   *Graphical abstract*

853